Journal of
Applied Remote Sensing

Estimating surface water area changes using time-series Landsat data in the Qingjiang River Basin, China

Zhiqiang Du
Bin Linghu
Feng Ling
Wenbo Li
Weidong Tian
Hailei Wang
Yuanmiao Gui
Bingyu Sun
Xiaoming Zhang

SPIE

Estimating surface water area changes using time-series Landsat data in the Qingjiang River Basin, China

Zhiqiang Du,[a] Bin Linghu,[b] Feng Ling,[c] Wenbo Li,[b] Weidong Tian,[d] Hailei Wang,[b] Yuanmiao Gui,[b] Bingyu Sun,[b] and Xiaoming Zhang[b]

[a]Wuhan University, State Key Laboratory of Information Engineering in Surveying, Mapping and Remote Sensing, No. 129 Luoyu Road, Wuhan, 430079, China

[b]Chinese Academy of Sciences, Institute of Intelligent Machines, No. 350 Shushanhu Road, Hefei, 230031, China

wbli@iim.ac.cn

[c]Chinese Academy of Sciences, Institute of Geodesy and Geophysics, No. 340 Xudong Road, Wuhan, 430077, China

[d]Hefei University of Technology, School of Computer and Information, No. 193 Tunxi Road, Hefei, 230009, China

Abstract. The Qingjiang River Basin, which is 423 km long in the Hubei province, China, is the first large tributary of the Yangtze River below the Three Gorges. The Qingjiang River Basin surface water area monitoring plays an important role in the water resource management strategy and regular monitoring management of the Yangtze River watershed. Hydropower cascade exploitation, which started in 1987, has formed three reservoirs including the Geheyan reservoir, the Gaobazhou reservoir, and the Shuibuya reservoir in the midstream and downstream of the Qingjiang River Basin. They have made a great impact on surface water area changes of the Qingjiang River Basin and need to be taken into account. We monitor the Qingjiang River Basin surface water area changes from 1973 to 2010. Ten scenes from the Multispectral Scanner System (MSS), seven scenes from the Thematic Mapper (TM), and two scenes from the Enhanced Thematic Mapper Plus (ETM+) remote sensing data of Landsat satellites, the normalized different water index (NDWI), the modified NDWI (MNDWI), and Otsu image segmentation method were employed to quantitatively estimate the Qingjiang River Basin surface water area in the 1970s, 1980s, 1990s, and 2000s, respectively. The results indicate that the surface water area of the Qingjiang River Basin shows a growing trend with the hydropower cascade development from the 1980s to the first decade of the 21st century. The study concluded the significance of human activities impact on surface water spatiotemporal distribution. Surface water accretion is significant in most parts of the Qingjiang River Basin and might be related to the constructed cascade hydropower dams. [DOI: 10.1117/1.JRS.6.063609]

Keywords: remote sensing; surface water; Qingjiang River Basin; dynamic change; Landsat.

Paper 12118 received May 1, 2012; revised manuscript received Nov. 4, 2012; accepted for publication Nov. 8, 2012; published online Nov. 28, 2012.

1 Introduction

Surface water is one of the irreplaceable strategic resources of human survival and social development.[1] It is essential for humans, their food crops, and ecosystems.[2] At the same time, land surface water is an important component of the water cycle. And water information extraction plays an important role in wetland inventory,[3–6] surface water survey and management,[7–14] flood monitoring and flood disaster risk assessment,[15–20] and environment monitoring.[21] Among the correlative research, surface water information extraction or the spatiotemporal change detection of surface water area is a key issue. In brief, the accurate extraction and measurement of water features and surface water area change is the most important study goal. Additionally, water

0091-3286/2012/$25.00 © 2012 SPIE

feature is one of the most important objects on the earth, and its extraction is of great significance to many related researches in remote sensing and hydrology domains. Over the past decades, multiresource remotely sensed data, such as the Thematic Mapper (TM),[1,2,7,17,22–25,26] the Enhanced Thematic Mapper Plus (ETM+),[3,5,25,27] the Systeme Probatoire d'Observation dela Tarre (SPOT),[4,6] the Multispectral Scanner System (MSS),[17] the Moderate-resolution Imaging Spectroradiometer (MODIS),[11,12,28] the Advanced Very High Resolution Radiometer (NOAA/AVHRR),[15–18] and the Small Satellite Constellation for Environment and Disaster Monitoring A/B (HJ-1A/B),[2,29] have been used to extract water features. Some widely used data are MSS, TM, and ETM+ images provided by Landsat series satellites. In the present study, the surface water area changes in the middle and lower reaches of the Qingjiang River Basin are estimated based on time series Landsat remote sensing images from 1973 to 2010.

2 Study Area and Data

2.1 *Study Area*

The Qingjiang River, which is 423 km long, is the first large tributary of the Yangtze River below the Three Gorges, in the Hubei province, China. The midstream and downstream of the Qingjiang River watershed was selected as the study area (Fig. 1). It is located between 30°22′–30°31′ N and 110°16′–111°24′ E. The Qingjiang River Basin has a moderate climate, an average annual rainfall of about 1400 mm, and an average flow of 440 m^3/s.[30] The Qingjiang River above Ziqiu town is a mountainous river with the river channel width ranging from 10 to 60 m in the dry period, and with most of the river flowing through the deep valleys with steep slopes of 60 to 80 deg on either side. On the other hand, the Qingjiang River below Ziqiu town is a half-mountainous river with the width of 60 to 100 m in the dry season. Three hydropower stations including Gaobazhou hydropower station, Geheyan hydropower station, and Shuibuya hydropower station have been built since 1987. In addition, three reservoirs including the Gaobazhou reservoir (from the Gaobazhou Dam to the Geheyan Dam, 50 km long), the Geheyan reservoir (from the Geheyan Dam to the Shuibuya Dam, 92 km long), and the Shuibuya reservoir (above the Shuibuya Dam, part of Shuibuya reservoir) have been formed. The land cover types of the study area include river, city, hydraulic structure, vegetation, soil, wetland, and mountain. The study area terrains are complicated, with mountains, foothills, and plains.

2.2 *Data*

Nineteen scenes from time-series Landsat satellites remote sensing data over the period of 1973 to 2010 archived from the U. S. Geological Survey server (http://earthexplorer.usgs.gov/) are used in this study (Table 1). The MSS sensors of Landsat-1 to Landsat-4 satellites have four bands of data with pixel resolution of 60 m from 0.5 to 1.1 μm. The Landsat-5 TM sensor has six bands of data with pixel resolution of 30 m from visible wavelengths to mid-infrared wavelengths. The ETM+ sensor of Landsat-7 also has six bands of data with pixel resolution of 30 m from 0.4 to 2.5 μm. All images used in the present paper are in the world reference system

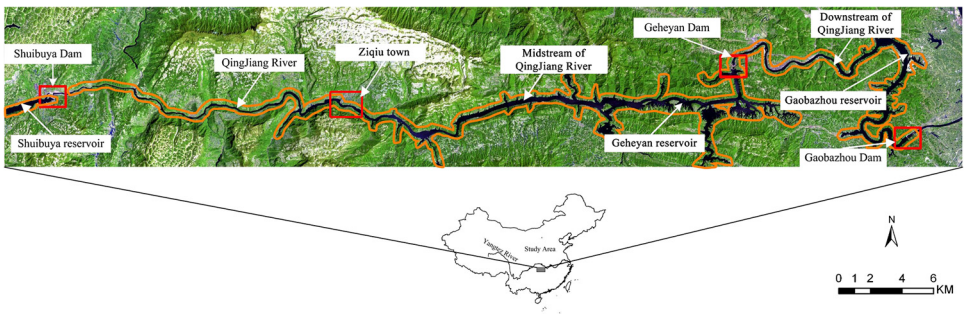

Fig. 1 Location of the study area. (Landsat-5 TM images false-color composite RGB: 753, 02 May 2010.)

Table 1 Specifications of MSS TM/ETM+ data used in this study.

Satellite	Sensor	Path/Row	Acq. date	Resolution (m)	Type	Producer	Wavelength (μm)
Lanssat-1	MSS	134/39	1973-11-22	60	GeoTiff	USGS	Band4: 0.50–0.60
Lanssat-2	MSS	134/39	1975-10-16				Band5: 0.60–0.70
			1977-06-01				Band6: 0.70–0.80
							Band7: 0.80–1.10
Lanssat-3	MSS	134/39	1979-05-31				
			1979-08-11				
			1979-11-09				
			1980-06-30				
Lanssat-4	MSS	125/39	1983-05-16	60	GeoTiff	USGS	Band1: 0.52–0.60
			1984-02-28				Band2: 0.63–0.69
			1984-06-03				Band3: 0.76–0.90
							Band4: 0.80–1.10
Lanssat-5	TM	125/39	1987-04-17	30	GeoTiff	USGS	Band1: 0.45–0.52
			1987-10-26				Band2: 0.52–0.60
			1993-09-24				Band3: 0.63–0.69
			1996-05-11				Band4: 0.76–0.90
			1996-10-18				Band5: 1.55–1.75
			2004-04-22				Band7: 2.08–2.35
			2010-05-02				
Lanssat-7	ETM+	125/39	1999-09-01	30	GeoTiff	USGS	Band1: 0.45–0.52
			2000-05-14				Band2: 0.53–0.61
							Band3: 0.63–0.69
							Band4: 0.77–0.90
							Band5: 1.55–1.75
							Band7: 2.09–2.35

(WGS84) datum with GeoTiff format, and are projected using the Universal Transverse Mercator system (zone UTM 49 North). Further information about the specifications of the satellite data used in the present study is given in Table 1.

3 Methods

Multisource remotely sensed images have been widely used in surface water assessment and management. These applications have involved water features delineation using the thematic information extraction techniques. Various information extraction methods have been proposed to extract water information from remotely sensed images.[6,22,23,27] In general, the methods of water information extraction can be divided into three categories: single-band method, classification method, and multiband method. A band image and a selected threshold are involved in the single-band method to extract water information, such as surface water area and its spatio-temporal distribution. However, the extracted water information is often mixed with the noises formed by different backgrounds, and the water information in some places will be miss-extracted. Supervised classifier and unsupervised classifier are usually adopted to extract surface water area. The result of water information from the classification method is more accurate compared with that coming from the single-band method. The multiband methods take advantage of the reflective differences of each involved band. Furthermore, multiband methods can be divided into two main kinds, such as the method with combination of multiband data and the ratio method. Compared with the single-band method, the multiband combination method proves more accurate extraction results, especially in the reduction of surface water information omitted extraction. The ratio method uses two multispectral bands of data to extract surface water distribution, and also demonstrated better accuracy and convenience when compared with other methods.[25,27] Therefore, two ratio water information extraction models, including normalized different water index (NDWI) and modified NDWI (MNDWI), have been employed to extract water information from remotely sensed data.[15–18,22–25,27,28]

3.1 *Ratio Water Features Extraction Model*

NDWI is one ratio method and is defined as follows:[22]

$$\mathrm{NDWI} = \frac{\mathrm{Green} - \mathrm{NIR}}{\mathrm{Green} + \mathrm{NIR}}, \tag{1}$$

where Green is a green channel image and NIR is a near infrared band image.

NDWI can achieve the following objectives: 1. maximize the reflectance of water by using green wavelengths and minimize the low reflectance of NIR by water features, and 2. take advantage of the high reflectance of NIR by vegetation and soil features.[25] As a result, the water feature value is more significant in the NDWI image, and the water information can be obtained with a suitable threshold.

The NDWI method can enhance water features information, but it cannot completely separate urban features from water features.[23,28] To address this problem, MNDWI has been developed and is defined as the following:[23]

$$\mathrm{MNDWI} = \frac{\mathrm{Green} - \mathrm{MIR}}{\mathrm{Green} + \mathrm{MIR}}, \tag{2}$$

where MIR is a mid-infrared band image.

The water information can also be obtained with a selected threshold from MNDWI.[23] Similar to NDWI, the MNDWI threshold value was set to zero.

3.2 *Image Threshold Segmentation*

Image segmentation is a key step in extracting water features information from NDWI or MNDWI data. The threshold segmentation has been adopted in NDWI and MNDWI to separate the image into two classes: water features and background features. The threshold values for NDWI and MNDWI were set to zero,[22,23] but the adjustment of the threshold based on actual situations is necessary. And that could achieve a more accurate result for the water information delineation.[23,28] Hence, dynamic thresholds are needed when different regions or different phases of remote sensing data are employed to detect water features information. Many methods can be used for image threshold segmentation.[28,31–34] The Otsu method[31] is a dynamic threshold method that has been successfully used in delineating water bodies and monitoring water area changes.[2,25] The Otsu method, an automatic thresholding segmentation algorithm, has been employed to determine the different thresholds for separating water features from the background features in the present study.

3.3 *Surface Water Area Estimation Model*

NDWI and MNDWI models have been successfully used in detecting water features information.[1–7,11,12,15–18,22–25,27–29] Nevertheless, we have found that there were different ratio water features extraction forms when MSS, TM, and ETM+ data were used. Especially for TM and ETM+ data, which band is selected for the NDWI or MNDWI method because there is one NIR band data (Band4: 0.77 to 0.90 μm) and two bands MIR data (Band5: 1.55 to 1.75 μm and Band7: 2.09 to 2.35 μm).

According to research results,[28] the ratio water features extraction model, which is composed of green spectral wavelength range of 0.52 to 0.60 μm and mid-infrared spectral wavelength range of 1.20 to 1.80 μm, is more suitable for water features information detection than that composed of green band and NIR band (0.76 to 0.90 μm) or mid-infrared band with the spectral wavelength range of 2.09 to 2.35 μm. Hence, Band4 and Band7 of Landsat-1 to Landsat-3 or Band1 and Band4 of Landsat-4 will be selected to form NDWI when MSS data are employed to extract water information. On the other hand, Band2 and Band5 of TM or ETM+ sensor will be used to structure MNDWI.

Therefore, we developed a five-step general procedure for using the MSS, TM, and ETM+ remote sensing images of Landsat satellites to estimate the surface water area based on NDWI or MNDWI. A flowchart of the proposed surface water area estimation model is shown in Fig. 2.

4 Results and Discussion

In our current research on the estimation of the surface water distribution area of the Qingjiang River Basin, China, we used NDWI and MNDWI as the primary tools. The surface water distribution area of the Qingjiang River Basin in the 1970s, 1980s, 1990s, and 2000s were estimated using the five-step general procedure mentioned above based on time series Landsat remote sensing data from 1973 to 2010. Then, the Qingjiang River Basin surface water distribution area changes of the 1970s, 1980s, 1990s, and 2000s were emphatically analyzed.

4.1 *Qingjiang River Basin Surface Water Area Estimation from 1973 to 2010*

Six scenes from MSS data, four scenes from MSS, and two scenes from TM data, two scenes from TM and one scene from ETM+ data, one scene from ETM+ and two scenes from TM data were selected to estimate the Qingjiang River Basin surface water area in the 1970s, 1980s, 1990s, and 2000s, respectively.

After data preprocessing, the subset of MSS, TM, and ETM+ data of Landsat satellites were used to extract water features information. Band4 and Band7 of Landsat-1 to Landsat-3 or Band1 and Band4 (Landsat-4) of the selected MSS data were used to generate original NDWI images using Eq. (1). Band2 and Band5 of the selected TM and ETM+ subset data were selected to generate original MNDWI images using Eq. (2).

We used the Otsu method and the original NDWI or MNDWI image to determine the initial thresholds. The threshold values had been adjusted to obtain the final image segmentation thresholds, according to the comparison of the water information extraction results with the reference data such as ETM+ Pan image or the same time RGB combinations of multispectral data. The final image segmentation thresholds were used to get water features distribution binary map. The Qingjiang River Basin surface water areas from 1973 to 2010 had been obtained by statistical analysis (Table 2).

When more than one scene of Landsat data were used in one year, the surface water area of the month, which was the same or close to the month of the other years in the same decade, was chosen to represent the surface water area of this year. For instance, November 1979, June 1984, and April 1987 were chosen to represent the surface water area of 1979, 1984, and 1987, respectively. Therefore, 14 years of surface water area were selected to show surface water area change trend of the Qingjiang River Basin from 1973 to 2010 (Fig. 3). Additionally, natural precipitation, as one of the important factors for surface water distribution change, can have an impact on the Qingjiang River Basin surface water change and therefore should be taken into consideration. Figure 3 shows the annual precipitation changes over the study period.[30] The maximum annual rainfall was more than 1800 mm (1983), while the minimum annual rainfall was about 1100 mm (1977), and the average annual rainfall was about 1400 mm.

From Fig. 3, the annual precipitation over the study period had some scale changes, while the Qingjiang River Basin surface water area made more dramatic shifts in different periods from 1973 to 2010. The changes from the 1970s to the 1980s and from the 1990s to the 2000s were more obvious. That makes it necessary to analyze the factors responsible for the surface water changes from the 1970s to the 1980s, which was the period before the hydropower cascade development of the Qingjiang River Basin, and these from the 1990s to the 2000s, which occurred after hydropower development. Hence, the following sections focus on the reasons for the surface water area changes of the Qingjiang River Basin before and after hydropower cascade development.

4.2 *Qingjiang River Basin Surface Water Area Changes Analysis from the 1970s to the 1980s*

Both natural precipitation and surface runoff in different seasons are uneven. This means that the Qingjiang River Basin surface water areas will have some changes in spring (March to May), summer (June to August), autumn (September to November), and winter (December to February of the next year). Consequently, it is necessary to analyze the surface water natural distribution of the study areas in different seasons before hydropower cascade exploitation. For this purpose,

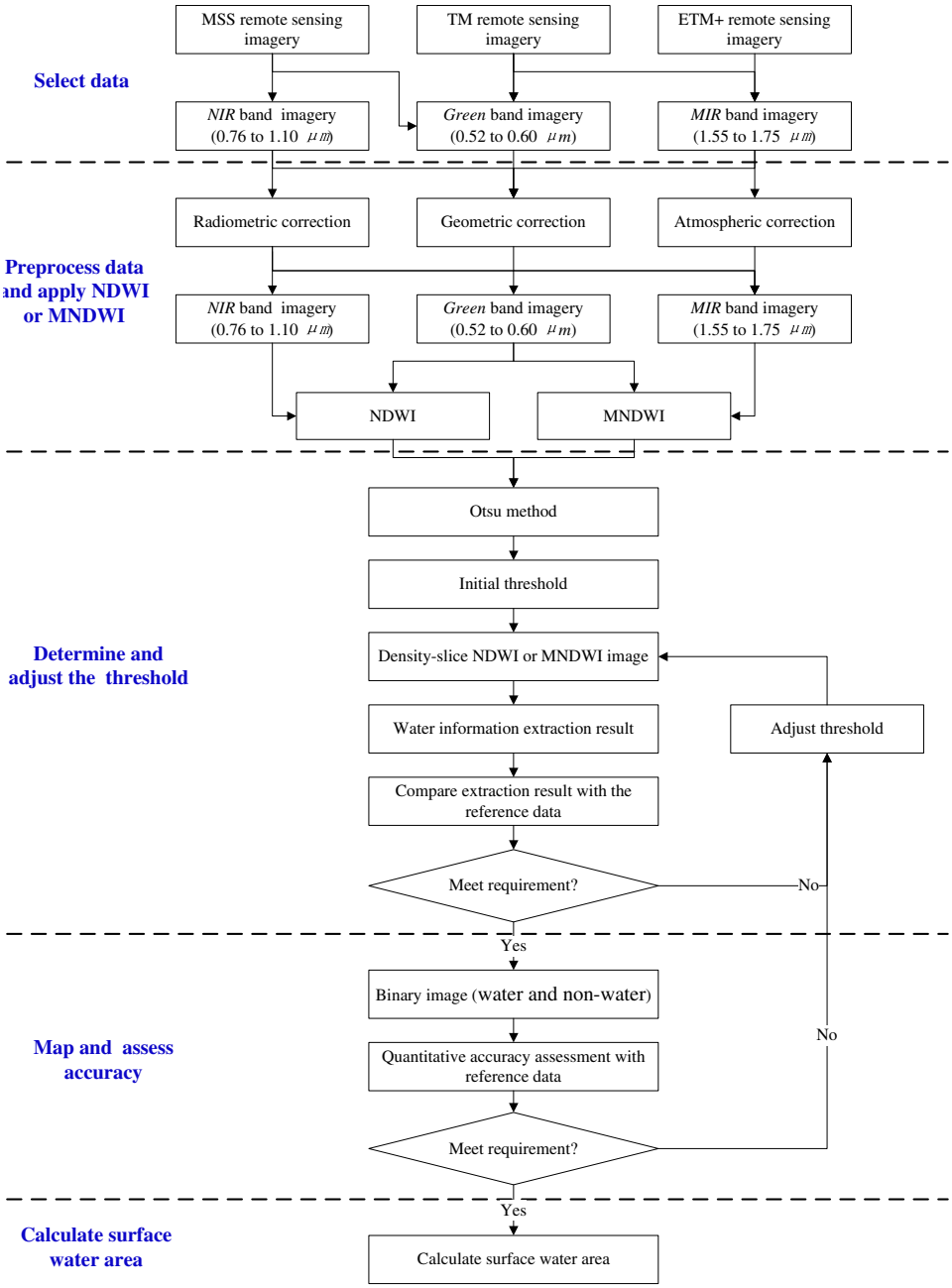

Fig. 2 Flowchart of the five-step surface water area estimation model.

two scenes of MSS remote sensing data, including Landsat-3 MSS data (May 1979), Landsat-4 MSS data (May 1983), and one scene of TM data (April 1987), were selected to estimate the Qingjiang River Basin surface water area in spring. Four scenes of MSS data (June 1977, Aug. 1979, June 1980, and June 1984) were chosen to estimate the surface water area in summer. Three scenes of MSS (November 1973, October 1975, and November 1979), and one scene TM (October 1987) data were employed to estimate the Qingjiang River Basin surface water area in autumn. One scene of MSS data (February 1984) were used to estimate surface water area in winter. In all, the selected twelve scenes of Landsat remote sensing data and the surface water area estimation model developed in this present paper were used to get the surface water spatiotemporal natural distribution in different seasons (Fig. 4).

From Fig. 4, the Qingjiang River Basin surface water spatiotemporal natural distributions had changes in different seasons, but the surface water areas from May to August were bigger than those from October to April of the next year. There were two reasons for that. First, the period from

Table 2 Statistical results, NDWI, MNDWI thresholds for the 1970s to the 2000s and associated sensors.

Time		Sensor	Threshold	Overall accuracy (%)	Overall Kappa	Area (km^2)
1970s	1973-11	MSS	0.301	93.67	0.8519	17.92
	1975-10		0.442	94.33	0.8709	17.32
	1977-06		−0.108	93.76	0.8586	33.44
	1979-05		−0.144	93.00	0.8523	35.36
	1979-08		−0.124	92.67	0.8466	30.61
	1979-11		0.141	93.67	0.8542	18.33
1980s	1980-06	MSS	0.004	94.00	0.8622	29.98
	1983-05		−0.093	92.33	0.8373	33.50
	1984-02		0.072	90.64	0.7996	15.31
	1984-06		−0.152	93.67	0.8628	32.04
	1987-04	TM	0.105	97.33	0.9443	17.79
	1987-10		0.286	95.99	0.9160	14.58
1990s	1993-09	TM	0.205	97.00	0.9376	48.62
	1996-10		0.198	97.33	0.9444	64.78
	1999-09	ETM+	0.257	97.67	0.9513	62.67
2000s	2000-05	ETM+	0.159	98.00	0.9582	48.57
	2004-04	TM	0.005	96.33	0.9235	62.56
	2010-05		0.002	97.76	0.9513	82.39

May to September belongs to the wet season, also known as the rainy season, making the precipitation during this stretch account for 75% to 78% of annual precipitation about 1400 mm (Fig. 3). Notably, the precipitation from May to August accounts for 50% to 55% of annual precipitation.[30] Second, seven months from October to April of the next year are in the dry season, and the runoff accounts for about 24% of the annual runoff. With these precipitation changes across the year, the width of the Qingjiang River Basin channel varies from 10 to 100 m in the dry season to 60 to 120 m in the wet season. Therefore, dividing the overall seasons into the wet and dry seasons to study Qingjiang Basin surface water changes is more suitable for a comprehensive view of the natural precipitation, surface runoff, and hydropower operation management.

Three scenes of Landsat data in autumn, including November 1973, October 1975, and November 1979, were selected to analyze the surface water area changes of the Qingjiang River Basin in the 1970s. The visual interpretation and overlay analysis with MSS false-color composite RGB: 756 indicated that NDWI images [Fig. 5(b), 5(d), and 5(f)] clearly showed water features as enhancement and some shadow regions were also enhanced. The reason is that the noise formed by the shadow has similar NDWI or MNDWI with water features.[24] Accuracy assessment results demonstrated that the results of the water features information extraction in the 1970s were consistent with the actual situation by comparison with the same time RGB combinations of MSS data. The overall accuracy and overall Kappa of the 1970s were more than 90% and 0.80 (Table 2). The accuracy assessment results also indicated that some small water boundaries had been mistakenly extracted because river channel width ranges from 10 to 100 m and MSS spatial resolution is 60 m. Results had the following indications. First, the Qingjiang River Basin surface water area was 17.92 km^2 in November 1973,

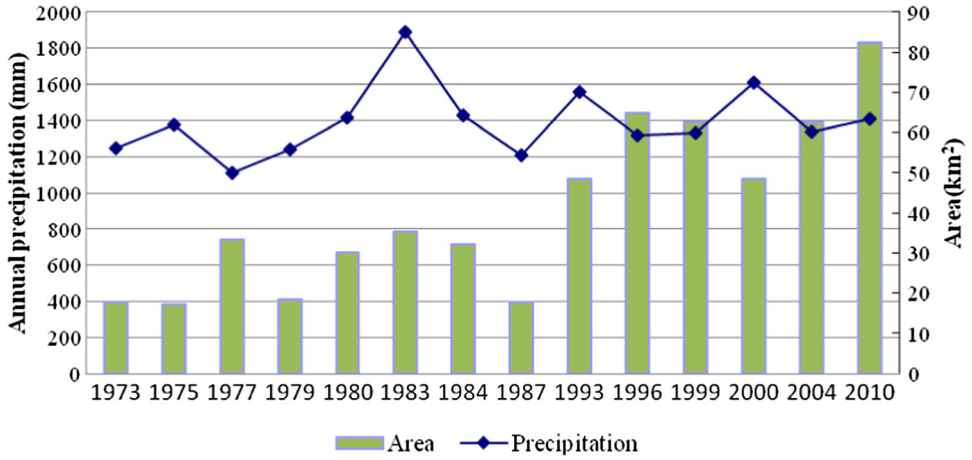

Fig. 3 Surface water area and annual precipitation changes of the Qingjiang River Basin from 1973 to 2010.

17.32 km^2 in October 1975, and 18.33 km^2 in November 1979. Second, the width of the midstream river varied from 10 to 60 m and that of the downstream shifted between 60 to 100 m over the three selected years. The reasons why the surface water area and the river width of 1973, 1975, and 1979 remained relatively stable are that the selected three scenes of MSS data were in the dry season, and the annual precipitation data over the period had slight changes (Fig. 3). This means that the surface water spatiotemporal distribution changes of the Qingjiang River Basin were mainly determined by natural precipitation in the 1970s.

When it came to the 1980s, three scenes of Landsat data, such as June 1980, June 1984, and April 1987, were chosen to analyze the reasons for the Qingjiang River Basin surface water area changes. The Qingjiang River Basin water features were enhanced by NDWI [Fig. 6(b) and 6(d)] and MNDWI [Fig. 6(f)] while the clouds also formed the noises [left and right side of Fig. 6(b)]. The mid and lower reaches surface water of the Qingjiang River Basin in 1980 and 1984 increased compared with the 1970s and 1987. The accuracy assessment results (Table 2) indicated that the water mapping accuracy from TM and MNDWI were higher than MSS and NDWI. Two reasons are responsible for that. First, TM spatial resolution, 30 m, is higher than MSS. Second, MNDWI is more suitable for water information extraction than NDWI.[23] Overall, the qualitative accuracy analysis and the quantitative accuracy assessment demonstrated that water

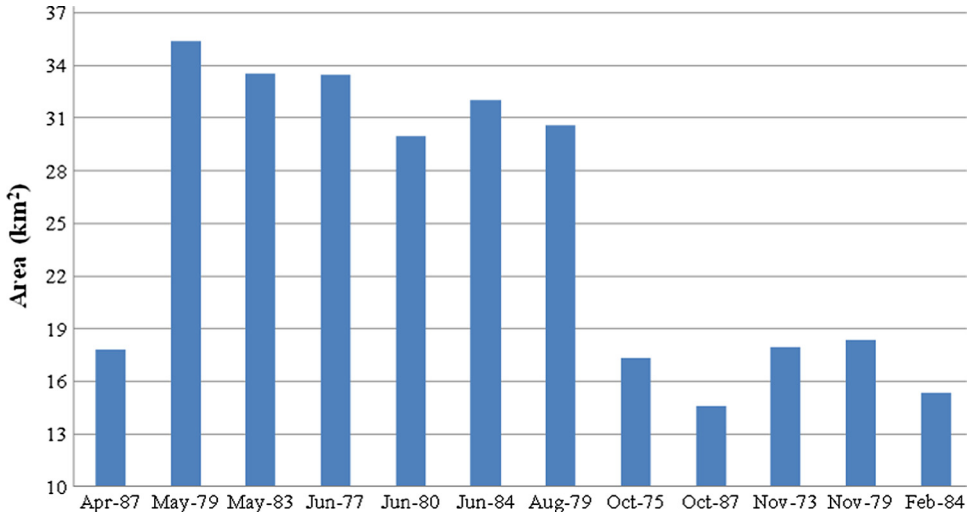

Fig. 4 Qingjiang River Basin surface water area distribution in different seasons.

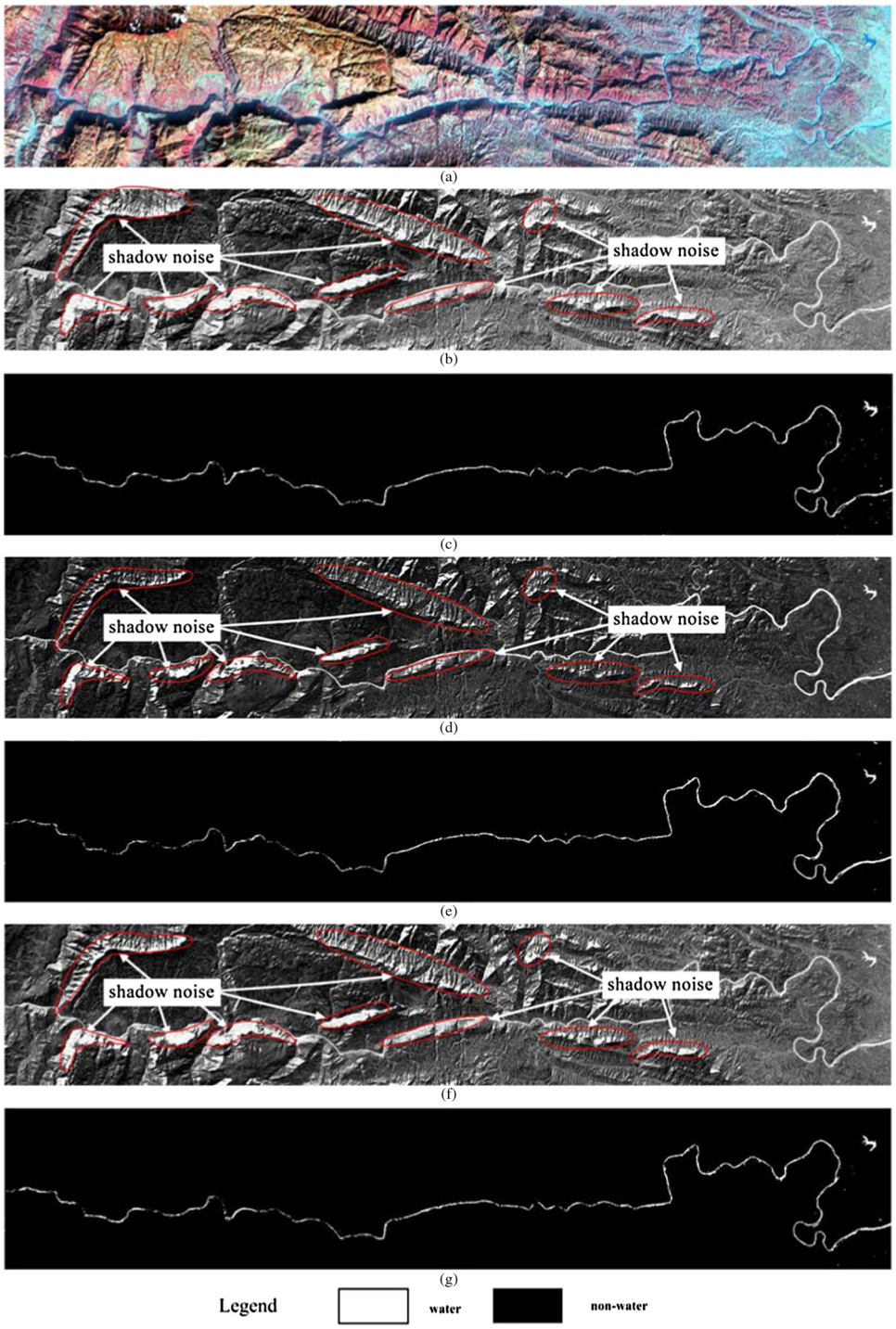

Fig. 5 Surface water distribution of the Qingjiang River Basin in the 1970s. (a) Landsat-1 MSS image (22 Nov. 1973) false-color composite (RGB: 754). (b) NDWI image of Nov. 1973. (c) Water/nonwater binary map derived from NDWI image of Nov. 1973. (d) NDWI image of Oct. 1975. (e) Water/nonwater binary map derived from NDWI image of Oct. 1975. (f) NDWI image of Nov. 1979. (g) Water/nonwater binary map derived from NDWI image of Nov. 1979.

features extraction results in the 1980s were consistent with the same time MSS and TM images. The results indicated [Fig. 6(c), 6(e), and 6(g)] that the main surface water of the study areas were detected, whereas some water features [middle side of Fig. 6(c)] were missing when cloud noises were removed. The surface water area of the study region was 29.98 km^2 (June 1980), 32.04 km^2 (June 1984), and 17.79 km^2 (April 1987).

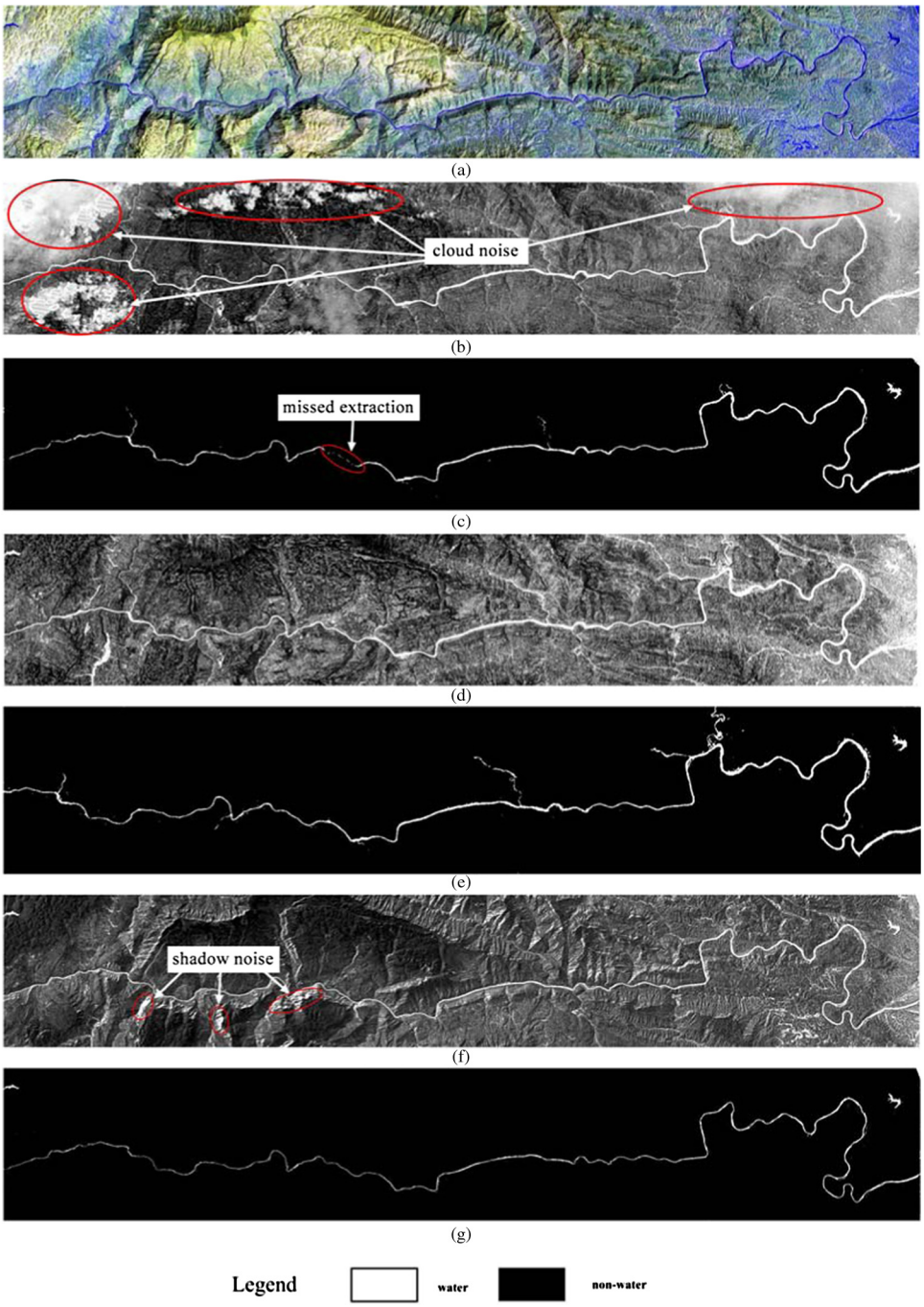

Fig. 6 Surface water distribution of the Qingjiang River Basin in the 1980s. (a) Landsat-5 TM image (17 Apr. 1987) false-color composite (RGB: 752). (b) NDWI image of Jun. 1980. (c) Water/nonwater binary map derived from NDWI image of Jun. 1980. (d) NDWI image of Jun. 1984. (e) Water/nonwater binary map derived from NDWI image of Jun. 1984. (f) MNDWI image of Apr. 1987. (g) Water/nonwater binary map derived from MNDWI image of Apr. 1987.

The river channel width in 1980 or 1984 was 60 to 120 m, which was wider than the range, from 10 to 100 m, in 1987. Two reasons can explain why the surface water area and the river width changes in 1980 or 1984 were more considerable than these in 1987. First, June 1980 and June 1984 were in the rainy season while April 1987 was in the dry season. Second, the annual precipitation data of 1980 and 1984 were bigger than that of 1987 (Fig. 3). In conclusion, the Qingjiang River Basin surface water spatiotemporal distribution changes were also mainly determined by the natural precipitation in the 1980s.

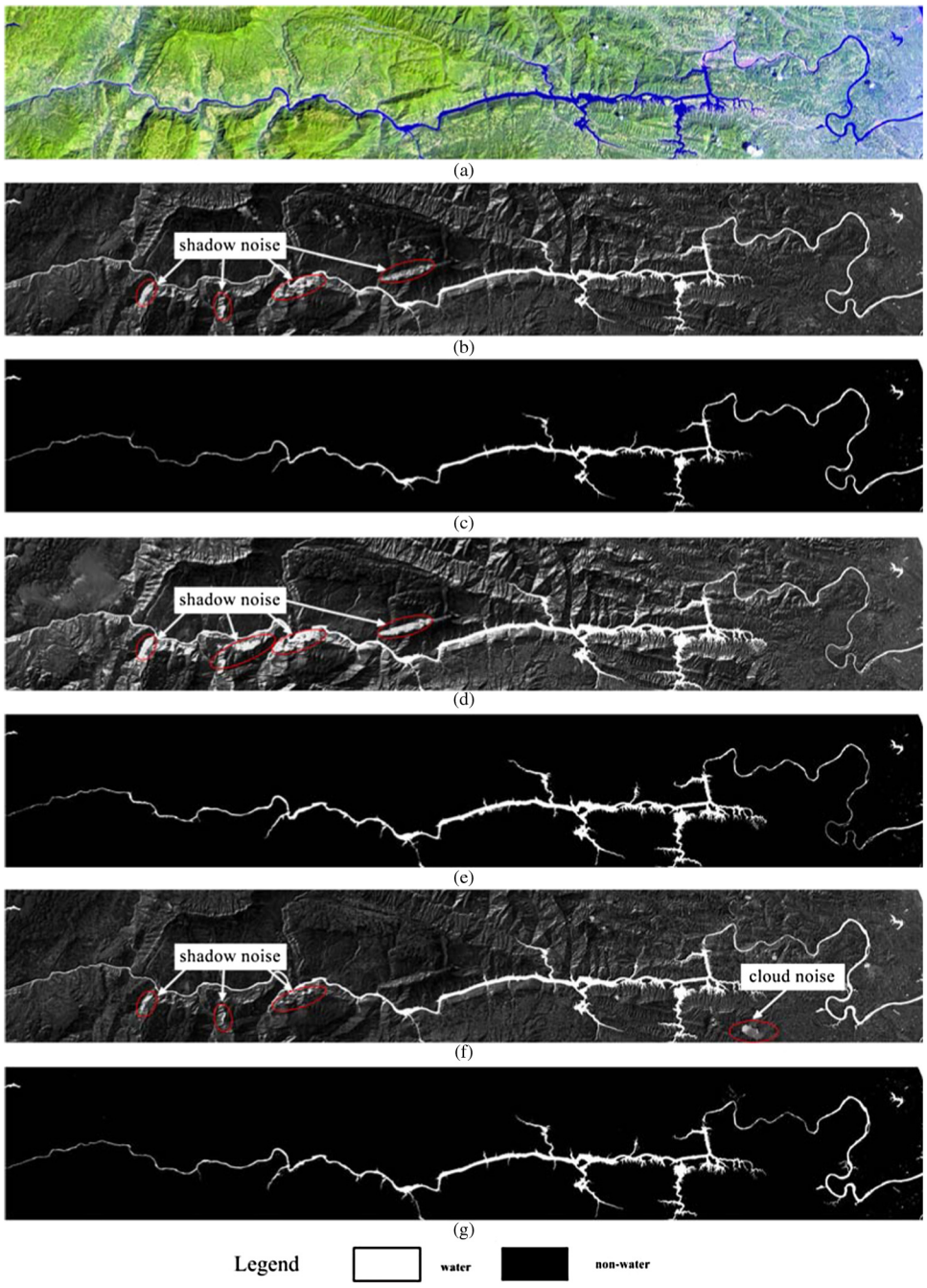

Fig. 7 Surface water distribution of the Qingjiang River Basin in the 1990s. (a) Landsat-7 ETM+ image (01 Sep. 1999) false-color composite (RGB: 751). (b) MNDWI image of Sep. 1993. (c) Water/nonwater binary map derived from MNDWI image of Sep. 1993. (d) MNDWI image of Oct. 1996. (e) Water/nonwater binary map derived from MNDWI image of Oct. 1996. (f) MNDWI image of Sep. 1999. (g) Water/nonwater binary map derived from MNDWI image of Sep. 1999.

4.3 *Qingjiang River Basin Surface Water Area Changes Analysis from the 1990s to the 2000s*

In this section, we focus on analyzing the Qingjiang River Basin surface water area changes after the hydropower cascade development. In the case of the 1990s, MNDWI images [Fig. 7(b), 7(d), and 7(e)] enhanced the water features but the clouds [lower right of Fig. 7(f)] and shadows [bottom left of Fig. 7(b), 7(d), and 7(f)] formed noise. The channels of the Qingjiang River

midstream-downstream in the 1990s were wider than in the 1980s. And, the midstream-downstream surface water area in the 1990s showed an increase compared with the 1980s. The overall accuracy and Kappa of the three selected years in the 1990s were higher than 97% and 0.93 (Table 2). Two reasons contributed to the greater overall accuracy in the quantitative assessment in the 1990s than that in the 1970s. First, TM/ETM+ data used in the 1990s have a higher resolution than MSS. Second, the channel width increased from the range of 10 to 100 m to 60 to 450 m due to the construction of two dams, the Geheyan Dam, which was started in 1987 and completed in 1993, and the Gaobazhou Dam, which was started in 1997 and completed in 1999. Overall, the water features information extraction results in the 1990s were consistent with the actual situation by comparison with the same time TM/ETM+ RGB (751) and panchromatic image. The Qingjiang River Basin surface water area was 48.62 km^2 in September 1993, 64.78 km^2 in October 1996, 62.67 km^2 in September 1999, and the river channel width increased to 60 to 450 m.

Although the selected TM and ETM+ data, September 1993 (TM), October 1996 (TM), and September 1999 (ETM+) were in the rainy season and the annual precipitation data of the three selected years in the 1990s had small changes (Fig. 3), the surface water spatiotemporal distribution of the study area in the 1990s had great changes. There are three reasons for that. First, the Geheyan reservoir stored more than 34 km^3 water for power generation from 1993 when the normal water level of the Geheyan Dam is 200 m. Second, the Gaobazhou reservoir also stored more than 4.3 km^3 water for power generation from 1999 when the normal water level of the Gaobazhou Dam is 80 m. Third, the river channel width of the study area increased from the range of 10 to 100 m to that of 60 to 450 m for the two formed reservoirs. From the above, we can draw the conclusion that the changes of the Qingjiang River Basin surface water spatiotemporal distribution in the 1990s were mainly determined by the hydropower cascade development.

In the 2000s (Fig. 8), the channels below the Geheyan Dam in 2004 and 2010 were wider compared with the 1990s and 2000. Similarly, the channel above the Shuibuya Dam in 2010 was wider than the 1990s, 2000, and 2004. Quantitative accuracy assessment demonstrated that the water features information extraction results in the 2000s were consistent with the actual situation by comparison with the same time RGB (453) of TM/ETM+ and ETM+ Pan data. The overall accuracy and Kappa of the 2000s were greater than 96% and 0.92 (Table 2). The Qingjiang River Basin surface water area was 48.57 km^2 in 2000, 62.56 km^2 in 2004, and 82.39 km^2 in 2010. The annual precipitation data of the three selected years in 2000s had slight changes (Fig. 3), whereas the Qingjiang River Basin surface water spatiotemporal distribution in the 2000s changed more substantially. There are three reasons behind that. First, the channels above the Shuibuya Dam in 2010 increased from 10 to 300 m because the Shuibuya reservoir stored about 5 km^3 the yield of water for power generation from 2006. However, it should be noted that only part of the Shuibuya reservoir has been focused on in this paper, and the total capacity of the Shuibuya reservoir should be more than 47 km^3. Second, the Gaobazhou reservoir released about 0.64 km^3 reservoir storage capacity for flood prevention in May 2000, which is in the flood period. Third, the Geheyan reservoir and the Gaobazhou reservoir stored more water for power generation in the dry season (April 2004). Finally, the conclusion can be reached that the Qingjiang River Basin surface water spatiotemporal distribution changes in the 2000s were mainly determined by the hydropower cascade development and hydropower scheduling operation.

From the above analyses, the annual precipitation from 1973 to 2010 had some changes but the Qingjiang River Basin surface water area was not more than 36 km^2 in the wet season before 1987 and it was more than 48 km^2 even in the dry season from 1993. Three main reasons are accountable for that. First, the Geheyan reservoir stored water for power generation from 1993. Second, the Gaobazhou reservoir stored water for power generation from 1999. Third, the Shuibuya reservoir stored water for power generation from 2006. It is necessary to analyze the upstream and downstream surface water area changes of the three reservoirs formed by the three dams.

4.4 *Analysis of the Upstream and Downstream Surface Water Changes of the Three Reservoirs*

In order to analyze the upstream and downstream surface water area changes of the three reservoirs, the same season Landsat data, such as MSS (May 1983, before the hydropower

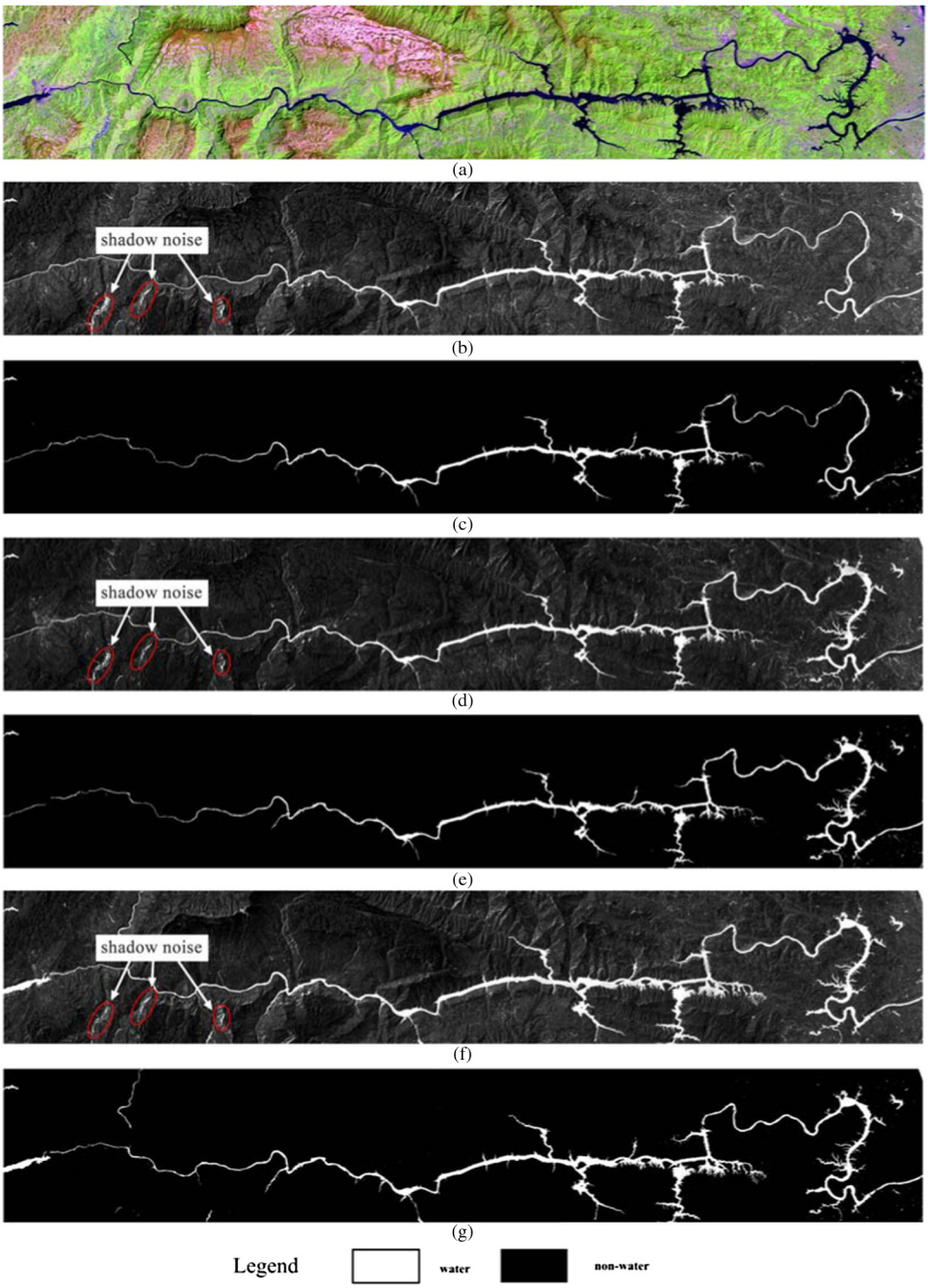

Fig. 8 Surface water distribution of the Qingjiang River Basin in the 2000s. (a) Landsat-5 TM images (02 May 2010) false-color composite (RGB: 542). (b) MNDWI image of May 2000. (c) Water/nonwater binary map derived from MNDWI image of May 2000. (d) MNDWI image of Apr. 2004. (e) Water/nonwater binary map derived from MNDWI image of Apr. 2004. (f) MNDWI image of May 2010. (g) Water/nonwater binary map derived from MNDWI image of May 2010.

cascade development), TM (May 1996, after the Geheyan Dam completion), ETM+ (May 2000, after the Gaobazhou Dam completion), and TM (May 2010, after the Shuibuya Dam completion), were selected. The surface water area changes of the three reservoirs are shown in Fig. 9.

From Fig. 9, the surface water area of the Shuibuya reservoir was not nearly 0.5 km^2 but increased to 3.25 km^2 in May 2010. This implies that the Shuibuya Dam had a significant impact on the spatiotemporal distribution of upstream surface water. Next, the Geheyan reservoir surface

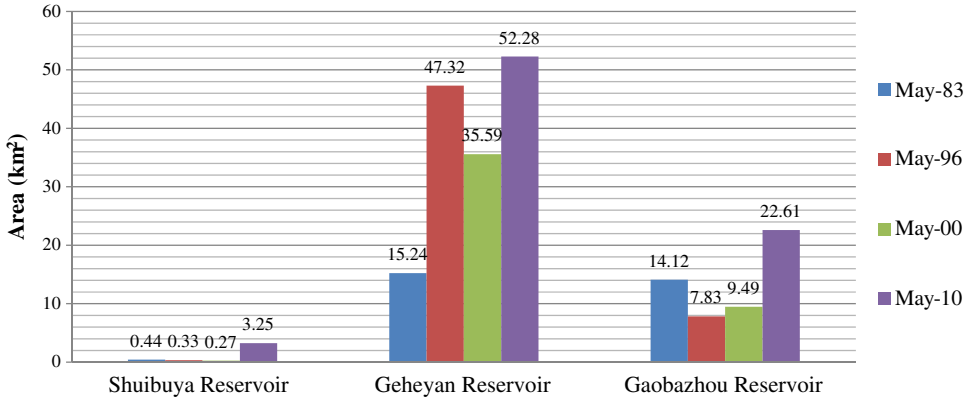

Fig. 9 Surface water area changes of the three reservoirs.

water area was 15.24 km^2 in May 1983 before the hydropower exploitation. It increased to 47.32 km^2 in 1996 because the Geheyan reservoir stored more than 34 km^3 water for power generation from 1993. However, it decreased to 35.59 km^2 in 2000 because the Geheyan reservoir released about 5 km^3 of reservoir storage capacity for flood prevention in the flood season (May to August). In 2010, it increased to 52.28 km^2 as the Geheyan reservoir stored more water for power generation due to the upstream Shuibuya reservoir sharing the Qingjiang River Basin flood pressure using operation scheduling. Finally, the Gaobazhou reservoir surface water area was 14.12 km^2 in May 1983, and decreased to 7.83 km^2 in 1996 because the upstream Geheyan reservoir started to store water, reducing the downstream natural runoff. However, it jumped up to 9.49 km^2 in May 2000 and soared to 22.61 km^2 in May 2010 when the Gaobazhou reservoir stored about 4.33 km^2 water for power generation from April 2000.

In general, three dams had great impacts on the upstream and downstream surface water areas distribution. The operation scheduling of the three reservoirs also did change surface water areas distribution. This means that the hydropower cascade development and the hydropower scheduling operation significantly influenced the spatiotemporal distribution of surface water distribution in the Qingjiang River Basin.

5 Conclusions

We calculated nineteen ratio water information extracting data (NDWI and MNDWI images) based on MSS, TM, and ETM+ time-series Landsat data of the Qingjiang River watershed from 1973 to 2010. The results show that: 1. the Qingjiang River Basin surface water area had little change from the 1970s to the 1980s and surface water area changes were mainly affected by natural precipitation before 1987; 2. the Qingjiang River Basin surface water area had relatively significant changes from the 1980s to the 1990s, especially in the midstream of the Qingjiang River Basin; 3. the Qingjiang River Basin surface water area had significant changes from the 1990s to the first decade of the 21st century, especially in the upstream and downstream; and 4. the main reasons for the increase of the Qingjiang River Basin surface water area were the hydropower cascade development and hydropower scheduling operation from 1987. The results indicate that the hydropower cascade exploitation in the Qingjiang River Basin had a significant impact on the surface water spatiotemporal distribution. The results also imply that NDWI and MNDWI can extract surface water area from Landsat data and they can be used to monitor surface water dynamic changes and detect flood disaster. Especially for estimating flood inundation area, the five-step general procedure developed in the present paper can be used to estimate the surface water area before flood and monitor flood inundation area during or after flood. The surface water area before flood and flood inundation area during flood can be used to get the flood affected area. Then different times flood affected area can be employed to conduct flood risk assessment and damage assessment with population data, crop data, road data, and other data.

Acknowledgments

This paper is financially supported by the National Natural Science Foundation of China (Nos. 41101516 and 91024008). The authors are indebted to the U.S. Geological Survey server (http://earthexplorer.usgs.gov/) for preprocessing and providing the MSS, TM, and ETM+ data used in this manuscript. The authors wish to thank Dr. Hongjie Xie, Associate Editor of Journal of Applied Remote Sensing, and two anonymous reviewers for their very constructive suggestions and comments. They also thank Miss Xiaoli Gong (Towson University) for revising the English of the manuscript.

References

1. M. K. Ridd and J. Liu, "A comparison of four algorithms for detection in an urban environment," *Remote Sens. Environ.* **63**(2), 95–100 (1998), http://dx.doi.org/10.1016/S0034-4257(97)00112-0.
2. S. Lu et al., "Water body mapping method with HJ-1A/B satellite imagery," *Int. J. Appl. Earth Obs. Geoinf.* **13**(3), 428–433 (2011), http://dx.doi.org/10.1016/j.jag.2010.09.006.
3. M. Ma et al., "Change in area of Ebinur Lake during the 1998–2005 period," *Int. J. Remote Sens.* **28**(24), 5523–5533 (2007), http://dx.doi.org/10.1080/01431160601009698.
4. J. Töyrä, A. Pietroniro, and L. W. Martz, "Multisensor hydrologic assessment of a freshwater wetland," *Remote Sens. Environ.* **75**(2), 162–173 (2001), http://dx.doi.org/10.1016/S0034-4257(00)00164-4.
5. G. Soliman and H. Soussa, "Wetland change detection in Nile swamps of southern Sudan using multitemporal satellite imagery," *J. Appl. Remote Sens.* **5**(1), 053517 (2011), http://dx.doi.org/10.1117/1.3571009.
6. A. Davranche, G. Lefebvre, and B. Poulin, "Wetland monitoring using classification trees and SPOT-5 seasonal time series," *Remote Sens. Environ.* **114**(3), 552–562 (2010), http://dx.doi.org/10.1016/j.rse.2009.10.009.
7. K. E. Sawaya et al., "Extending satellite remote sensing to local scales: land and water resource monitoring using high-resolution imagery," *Remote Sens. Environ.* **88**(1–2), 144–156 (2003), http://dx.doi.org/10.1016/j.rse.2003.04.006.
8. X. Ding and X. Li, "Monitoring of the water-area variations of Lake Dongting in China with ENVISAT ASAR images," *Int. J. Appl. Earth Obs. Geoinf.* **13**(6), 894–901 (2011), http://dx.doi.org/10.1016/j.jag.2011.06.009.
9. P. K. Singh, S. Kumar, and U. C. Singh, "Groundwater resource evaluation in the Gwalior area, India, using satellite data: an integrated geomorphological and geophysical approach," *Hydrogeol. J.* **19**(7), 1421–1429 (2011), http://dx.doi.org/10.1007/s10040-011-0758-6.
10. A. I. J. M. Van Dijk and L. J. Renzullo, "Water resource monitoring systems and the role of satellite observations," *Hydrol. Earth Syst. Sci.* **15**(1), 39–55 (2011), http://dx.doi.org/10.5194/hess-15-39-2011.
11. C. Giardino et al., "Application of remote sensing in water resource management: the case study of Lake Trasimeno, Italy," *Water Resour. Manage.* **24**(14), 3885–3899 (2010), http://dx.doi.org/10.1007/s11269-010-9639-3.
12. Y. Huang et al., "Integrated modeling system for water resources management of Tarim River Basin," *Environ. Eng. Sci.* **27**(3), 255–269 (2010), http://dx.doi.org/10.1089/ees.2009.0359.
13. B. Nishat and S. M. M. Rahman, "Water resources modeling of the Ganges-Brahmaputra-Meghna River Basins using satellite remote sensing data," *J. Am. Water. Resour. Assoc.* **45**(6), 1313–1327 (2009), http://dx.doi.org/10.1111/jawr.2009.45.issue-6.
14. E. Dimitrioua and I. Zachariasb, "Applying isotopic techniques and remote sensing for water resources management an a lake catchment," *Water Int.* **32**(3), 457–474 (2007), http://dx.doi.org/10.1080/02508060708692224.
15. I. J. Barton and J. M. Bathols, "Monitoring floods with AVHRR," *Remote Sens. Environ.* **30**(1), 89–94 (1989), http://dx.doi.org/10.1016/0034-4257(89)90050-3.
16. Y. Sheng, P. Gong, and Q. Xiao, "Quantitative dynamic flood monitoring with NOAA AVHRR," *Int. J. Remote Sens.* **22**(9), 1709–1724 (2001), http://dx.doi.org/10.1080/01431160118481.

17. J. Zhang et al., "Flood disaster monitoring and evaluation in China," *Environ. Hazards* **4**(2–3), 33–43 (2002), http://dx.doi.org/10.1016/S1464-2867(03)00002-0.
18. R. G. Bryant and M. P. Rainey, "Investigation of flood inundation on playas within the Zone of Chotts, using a time-series of AVHRR," *Remote Sens. Environ.* **82**(2–3), 360–375 (2002), http://dx.doi.org/10.1016/S0034-4257(02)00053-6.
19. J. Sanyal and X. Lu, "Application of remote sensing in flood management with special reference to monsoon Asia: a review," *Nat. Hazards* **33**(2), 283–301 (2004), http://dx.doi.org/10.1023/B:NHAZ.0000037035.65105.95.
20. H. Qi and M. S. Altinakar, "Simulation-based decision support system for flood damage assessment under uncertainty using remote sensing and census block information," *Nat. Hazards* **59**(2), 1125–1143 (2011), http://dx.doi.org/10.1007/s11069-011-9822-8.
21. J. Amanollahi et al., "PM10 monitoring using MODIS AOT and GIS in Kuala Lumpur, Malaysia," *Res. J. Chem. Environ.* **15**(2), 982–985 (2011).
22. S. M. McFeeters, "The use of the normalized difference water index (NDWI) in the delineation of open water features," *Int. J. Remote Sens.* **17**(7), 1425–1432 (1996), http://dx.doi.org/10.1080/01431169608948714.
23. H. Xu, "Modification of normalized difference water index (NDWI) to enhance open water features in remotely sensed imagery," *Int. J. Remote Sens.* **27**(14), 3025–3033 (2006), http://dx.doi.org/10.1080/01431160600589179.
24. W. Li and Q. Zhang, "Water extraction based on self-fusion of ETM+ remote sensing data and normalized ration index," *Proc. SPIE* **6419**, 641911 (2006), http://dx.doi.org/10.1117/12.713010.
25. F. Karsli, A. Guneroglu, and M. Dihkan, "Spatio-temporal shoreline changes along the southern Black Sea coastal zone," *J. Appl. Remote Sens* **5**(1), 053545 (2011), http://dx.doi.org/10.1117/1.3624520.
26. F. Sun et al., "Comparison and improvement of methods for identifying waterbodies in remotely sensed imagery," *Int. J. Remote Sens.* **33**(21), 6854–6875 (2012), http://dx.doi.org/10.1080/01431161.2012.692829.
27. C. Qiao et al., "An adaptive water extraction method from remote sensing image based on NDWI," *J. Ind. Soc. Remote Sens.* **40**(3), 421–433 (2012), http://dx.doi.org/10.1007/s12524-011-0162-7.
28. L. Ji, L. Zhang, and B. Wylie, "Analysis of dynamic thresholds for the normalized difference water index," *Photogramm. Eng. Remote Sens.* **75**(11), 1307–1317 (2009).
29. F. Ling et al., "Monitoring river discharge with remotely sensed imagery using river island area as an indicator," *J. Appl. Remote Sens.* **6**(1), 063564 (2012), http://dx.doi.org/10.1117/1.JRS.6.063564.
30. C. Zhu, M. He, and A. Ma, "The variation characteristic of rainfall of Qingjiang River Basin under the global climate warming," *Hydropower New Energ.* **3**, 49–51 (2011) (In Chinese).
31. N. Otsu, "A threshold selection method from gray-level histograms," *IEEE Trans. Syst. Man Cybern.* **9**(1), 62–69 (1979), http://dx.doi.org/10.1109/TSMC.1979.4310076.
32. N. Ramesh, J.-H. Yoo, and I. K. Sethi, "Thresholding based on histogram approximation," *IEE Proc. Vis. Image Signal Process.* **142**(5), 271–279 (1995), http://dx.doi.org/10.1049/ip-vis:19952007.
33. C. V. Jawahar, P. K. Biswas, and A. K. Ray, "Investigations on fuzzy thresholding based on fuzzy clustering," *Pattern Recogn.* **30**(10), 1605–1613 (1997), http://dx.doi.org/10.1016/S0031-3203(97)00004-6.
34. M. Cheriet, J. N. Said, and C. Y. Suen, "A recursive thresholding technique for image segmentation," *IEEE Trans. Image Process.* **7**(6), 918–921 (1998), http://dx.doi.org/10.1109/83.679444.

Biographies and photographs of the authors not available.